



# Geochemical modeling of CO<sub>2</sub> injection and gypsum precipitation at the Ketzin CO<sub>2</sub> storage site

Eunseon Jang<sup>1</sup> · Bernd Wiese<sup>1</sup> · Peter Pilz<sup>1</sup> · Sebastian Fischer<sup>2</sup> · Cornelia Schmidt-Hattenberger<sup>1</sup>

Received: 5 June 2021 / Accepted: 12 February 2022  
© The Author(s) 2022

## Abstract

Gypsum crystals are found at the well perforation of observation well Ktzi 202 of the test site for CO<sub>2</sub> storage at Ketzin, Germany. XRD analysis confirms pure gypsum. Fluid samples before and after CO<sub>2</sub> injection are analyzed. Geochemical modeling is conducted to identify the mechanisms that lead to gypsum formation. The modeling is carried out with PHREEQC and Pitzer database due to the high salinity of up to 5 mol per kg water. Due to their significantly higher reactivity compared to other minerals like silicates, calcite, dolomite, magnesite, gypsum, anhydrite, and halite are considered as primary mineral phases for matching the observed brine compositions in our simulations. Calcite, dolomite, and gypsum are close to saturation before and after CO<sub>2</sub> injection. Dolomite shows the highest reactivity and mainly contributes to buffering the brine pH that initially decreased due to CO<sub>2</sub> injection. The contribution of calcite to the pH-buffering is only minor. Gypsum and anhydrite are no geochemically active minerals before injection. After CO<sub>2</sub> injection, gypsum precipitation may occur by two mechanisms: (i) dissociation of CO<sub>2</sub> decreases activity of water and, therefore, increases the saturation of all minerals and (ii) dolomite dissolution due to pH-buffering releases Ca<sup>2+</sup> ions into solution and shifts the mass action to gypsum. Gypsum precipitation decreases with increasing temperature but increases with increasing partial CO<sub>2</sub> pressure. Our calculations show that calcium sulfate precipitation increases by a factor of 5 to a depth of 2000 m when Ketzin pressure and temperature are extrapolated. In general, gypsum precipitation constitutes a potential clogging hazard during CO<sub>2</sub> storage and could negatively impact safe site operation. In the presented Ketzin example, this threat is only minor since the total amount of gypsum precipitation is relatively small.

**Keywords** Carbon capture and storage · Ketzin CO<sub>2</sub> storage site · Calcium sulfate mineral precipitation · Geochemical modeling

## Introduction

The assessment of potential mineral precipitation is essential for the safety demonstration of the permanent CO<sub>2</sub> storage project. The injection of CO<sub>2</sub> into the reservoir disturbs the geochemical equilibrium. Injected CO<sub>2</sub> dissolves into the reservoir brine and lowers the brine pH. Subsequently, acid-induced reactions may occur, namely dissolution of primary minerals and precipitation of secondary minerals. The mineral precipitation, especially precipitation of carbon-bearing minerals in reservoir formations, is generally favorable for the long-term safety of the geologic CO<sub>2</sub> storage operation. However, dissolution or precipitation of minerals may change the physical properties, such as permeability and porosity, and chemical compositions of the reservoir (Labus and Wertz 2017; Rendel et al. 2016).

---

✉ Eunseon Jang  
ejang@gfz-potsdam.de

Bernd Wiese  
wiese@gfz-potsdam.de

Peter Pilz  
peter.pilz@gfz-potsdam.de

Sebastian Fischer  
Sebastian.Fischer@bgr.de

Cornelia Schmidt-Hattenberger  
cornelia.schmidt-hattenberger@gfz-potsdam.de

<sup>1</sup> 4.8 Geoenergy, GFZ German Research Centre for Geosciences, Telegrafenberg, 14473 Potsdam, Germany

<sup>2</sup> Federal Institute for Geosciences and Natural Resources (BGR), Wilhelmstr. 25-30, 13593 Berlin, Germany

Moreover, the secondary mineral precipitation possibly clogs the well-bore and surrounding areas, which may decrease CO<sub>2</sub> injectivity during the injection phase, causing a negative impact on project operations (Bacon et al. 2009; Rosenberg et al. 2012). To prevent undesired mineral precipitation, scale inhibitors are often added to the brine solution in many industrial processes. However, the inhibitors containing chemicals may have harmful effects on the environment and increase operating costs (Lattemann and Höpner 2008; Reiss et al. 2021).

Secondary calcium sulfate mineral precipitation may be relevant for storage operation, mainly due to its clogging potential. In the presence of high concentrations of calcium and sulfate ions in the brine, the calcium sulfate mineral (e.g., gypsum or anhydrite) can precipitate (Garcia-Rios et al. 2015; Rendel et al. 2016). This reaction is potentially important at the Ketzin CO<sub>2</sub> storage site in Germany. Compared to other CO<sub>2</sub> storage sites, the Ketzin site shows a relatively high calcium and sulfate concentration in the reservoir brine (Table 1).

The mineralogical–geochemical reactions due to CO<sub>2</sub> injection have been studied for specific rock specimen by laboratory experiments (Fischer et al. 2013; Garcia-Rios et al. 2014), field monitoring (Emberley et al. 2004; Förster et al. 2019; Wiese et al. 2013), and modeling tools (Bacon et al. 2009; De Lucia et al. 2012; Gaus et al. 2005). The induced changes in rock volume, brine composition, and the mineral CO<sub>2</sub> trapping capacity under CO<sub>2</sub> conditions have been investigated by different authors (Klein et al., 2013; Kühn et al. 2013; Tremosa et al. 2014; Xu et al. 2003). Specifically, to predict the potential precipitation of mineral phases under CO<sub>2</sub> storage conditions, an understanding of the mineral thermodynamic properties is necessary. Different studies investigate the solubility of calcium sulfate with experiments and modeling in natural and synthetic solutions (Arslan and Dutt 1993; Dai et al. 2017; Reznik et al. 2011), but only a few studies consider

the presence of high CO<sub>2</sub> concentrations (Reiss et al. 2021; Rendel et al. 2016; Wolfe and Bennett 2011).

This work aims to investigate the mineral precipitation at the Ketzin CO<sub>2</sub> storage site with field monitoring and geochemical batch modeling. Samples affected by five years of CO<sub>2</sub> exposition were retrieved during a back-production experiment and analyzed by means of a geochemical model for the first time. Also, the analysis of precipitated minerals in a reservoir observation well is presented for the first time.

## Study area

### Ketzin CO<sub>2</sub> storage site

#### Location and CO<sub>2</sub> injection

The Ketzin CO<sub>2</sub> storage site is located in the Northeast German Basin (NEGB), about 25 km west of Berlin, Germany [Fig. 1(a)]. A total of five wells had been installed, comprising three reservoir observation wells (Ktzi 200, Ktzi 202, and Ktzi 203), one reservoir injection/observation well (Ktzi 201), and one above reservoir observation well (P300). The injection/observation well (Ktzi 201) and two observation wells (Ktzi 200 and Ktzi 202) were drilled in 2007, and the third observation well (Ktzi 203) was drilled in 2012, all to depths of 700–800 m. The additional shallow observation well (P300) was drilled in 2011 to a depth of 450 m ca. 25 m north-west from the observation well Ktzi 202 to monitor possible hydraulic and geochemical impacts of the injected CO<sub>2</sub> on the groundwater of the shallower aquifer overlying the reservoir and the cap-rock zone. The spatial layout is shown in Fig. 1(b).

From June 2008 to August 2013, CO<sub>2</sub> was injected at a depth of 630–650 m into the porous sandstone reservoir of the Upper Triassic Stuttgart Formation. The injected CO<sub>2</sub> had mainly a purity > 99.9%, and only from May to June 2011, 1.515 kt CO<sub>2</sub> with a slightly reduced purity

**Table 1** Reservoir brine composition, baselines prior to CO<sub>2</sub> injection in CCS storage sites

	Ketzin (Germany)	In Salah (Algeria)	Weyburn (Canada)	Cranfield (USA)	Rose Run (USA)
pH	6.4	5.2	6.0	7.7	6.4
Na (mol/kg)	4.93E+00	1.87E+00	1.18E+00	1.05E+00	2.62E+00
K (mol/kg)	1.37E-02	6.98E-03	1.05E-02	1.80E-02	8.58E-02
Ca (mol/kg)	6.77E-02	6.78E-01	3.68E-02	3.47E-02	9.38E-01
Mg (mol/kg)	4.34E-02	2.63E-01	1.65E-02	1.64E-04	2.42E-01
Cl (mol/kg)	4.90E+00	3.77E+00	1.17E+00	1.06E+00	5.39E+00
SO <sub>4</sub> (mol/kg)	5.25E-02	8.28E-03	3.88E-02	1.32E-09	3.40E-03
HCO <sub>3</sub> (mol/kg)	1.82E-03	3.52E-03	4.82E-03	8.96E-04	2.00E-03
TDS (mol/kg)	1.00E+01	6.60E+00	2.45E+00	2.16E+00	9.28E+00
References	Würdemann et al. (2010)	Tremosa et al. (2014)	Emberley et al. (2004)	Xu et al. (2003)	Breen et al. (1985)

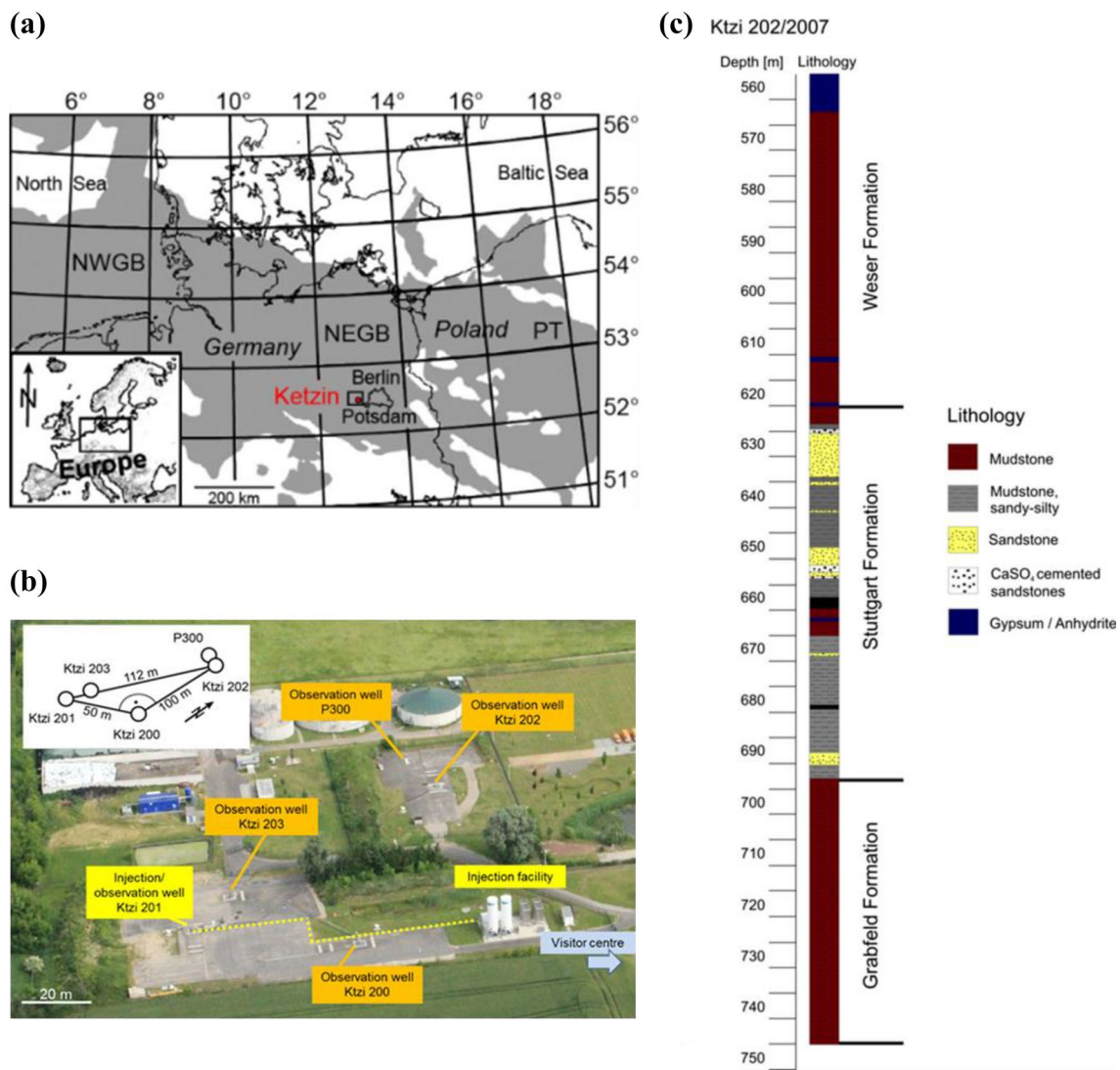


**Fig. 1** **a** Location of the Ketzin site. NWGB, NEGB, and PT refer to the Northwest German Basin, Northeast German Basin, and Polish Trough, respectively. **b** Aerial view of the pilot site in Ketzin in August 2013. The five wells are arranged in a triangular shape with

approx. 50–100 m away from each other. **c** Lithostratigraphic column of the observation well Ktzi 202, modified after Norden and Frykman (2013)

of > 99.7%. The gas consisted of CO<sub>2</sub> with traces of N<sub>2</sub>, He, and CH<sub>4</sub> (Liebscher et al. 2013). After the injection of 67 kt CO<sub>2</sub>, the site entered into the post-injection phase. The abandonment phase started in 2013 with a staged abandonment of the observation well Ktzi 202. Ktzi 202 was finally abandoned in 2015, and all other wells were finally abandoned in 2017, not available anymore for post-injection monitoring. More details concerning the site and storage operation can be found in Würdemann et al. (2010), Möller et al. (2012), and Martens et al. (2014) and abandonment of a storage site Prevedel et al. (2014).

**Geological setting**

The Ketzin storage site is located in the Ketzin part of the Roscow-Ketzin double-anticline, and it provides a classical multi-barrier system. The target reservoir for CO<sub>2</sub> storage is a 6–15 m thick sandstone reservoir, located in the Triassic Stuttgart Formation with 80 m thick interbedded mud- and sandstone. About 5 m above the reservoir, the Weser Formation starts (up to 165 m thick clay- and mudstone) and acts as cap-rock [Fig. 1(c)]. The Stuttgart Formation is lithologically highly heterogeneous and composed of sandstone with high permeability and good reservoir properties and

siltstone interbedded with mudstone that has lower permeability and poor reservoir properties (Norden and Frykman 2013). The chemical composition of the sandstone is mainly composed of quartz (24–41 wt%), plagioclase (16–35 wt%), illite + muscovite (10–30 wt%), and k-feldspar (6–13 wt%) in the pristine reservoir sandstone samples. Analcime (0–11 wt%), anhydrite + gypsum (0–37 wt%), and dolomite (0–3 wt%) occur as pore-filling cement phases. Specifically, the evaporite minerals, such as anhydrite and gypsum, were deposited from supersaturated hypersaline and sulfate-rich brine during early diagenetic processes (Kasina et al., 2017) [Fig. 1(c)]. The porosity varies between 13 and 26%, and the pump test permeability is 40–110 mD (Wiese et al. 2010). Multi-physical modeling shows a spatial permeability distribution mainly between 50 and 300 mD close to the wells (Wagner and Wiese 2018). A detailed description of the local geology can be found in Förster et al. (2019) and Norden and Frykman (2013).

### Brine composition

The initial reservoir brine was characterized before CO<sub>2</sub> injection. As shown in Table 2, four initial brine samples were obtained during a lift test after completing the observation well Ktzi 202 in 2008 (Würdemann et al. 2010). The average composition of the brine samples before the CO<sub>2</sub> injection is referred to as baseline composition (B) in this work. The baseline fluid has an average total dissolved solids (TDS) content of 234.76 g/L with a pH value of 6.53. The B brine is a pronounced Na–Cl water type with a noticeable amount of calcium (Ca<sup>2+</sup>) and sulfate (SO<sub>4</sub><sup>2-</sup>).

In 2014, one year after finishing the five-year CO<sub>2</sub> injection period, a back-production experiment was conducted. A total amount of 240 tons of CO<sub>2</sub> and 55 m<sup>3</sup> of reservoir brine

were back-produced from the injection/observation well Ktzi 201. The experiment aimed to investigate (i) reservoir and well-bore behavior during back-production of CO<sub>2</sub>, (ii) composition of the retrieved gas, and (iii) the distribution of the released gas in the atmosphere (Martens et al. 2015). Ten fluid samples were taken and analyzed as listed in Table 3 [Pers. Comm. Martin Zimmer (GFZ)]. The large amount of brine and the high flow rate imply that near-well effects do not bias the samples, wherefore we consider the samples as very representative. The arithmetic average of these analyses is the post-injection brine composition (PI) in this study. The average TDS of the PI is 235.44 g/L, which is similar to that of the B brine, but the pH value of 6.18 is slightly lower than for the baseline. The PI brine remains a Na–Cl water type.

### Reservoir temperature and pressure changes

During the CO<sub>2</sub> injection at the Ketzin site, the reservoir temperature and pressure were measured using a fiber optic permanent downhole gauge (Liebscher et al. 2013; Prevedel et al. 2009). The Ketzin reservoir pressure and temperature conditions (p–T conditions) were changed during the operation phases, such as phases of low and high injection rates, shut-in, and re-start operations (Liebscher et al. 2013).

The reservoir p–T conditions are available at the observation well Ktzi 202 from March 2008 till October 2011 (previously unpublished observation data). The temperature and pressure data are used to construct the p–T diagram at a depth of 650 m. Before the CO<sub>2</sub> injection started (30 June 2008), the initial reservoir condition was 34.5 °C/63.5 bar at a depth of 650 m in well Ktzi 202 (09 June 2008). During the CO<sub>2</sub> injection, the reservoir pressure rose about 10 to 13 bars above the initial reservoir pressure. After injection stopped, the pressure slowly decreased and smoothly approached the initial pressure conditions again (Wipki et al. 2016). The temperature changes in the well are induced by evaporation and condensation of CO<sub>2</sub>, also called the heat-pipe effect (Henninges et al. 2011). The forming of the heat pipe is affected by different factors, e.g., recent pressure changes that may be induced by injection rate changes or well pressure variations induced by the wireline sampling itself.

Immediately before the back-production experiment, the reservoir pressure was about 65.5 bar at the well Ktzi 201, used to recalculate reservoir equilibrium for post-injection conditions (PI). Further information on the reservoir pressure and temperature changes at the full-lifecycle are kindly referred to, e.g., Henninges et al. (2011), Liebscher et al. (2013), and Wipki et al. (2016).

### Field observations/investigations

Video camera inspections were conducted for screening the inner surface of the well-bore casing as a part of the well

**Table 2** Baseline fluid composition (B) from the observation well Ktzi 202 (Würdemann et al. 2010)

Parameter	B-1	B-2	B-3	B-4
Date	8.1.2008	9.1.2008	9.1.2008	10.1.2008
pH	6.70	6.50	6.50	6.40
Na <sup>+</sup> (mg/L)	8.74E+04	9.04E+04	8.84E+04	9.04E+04
K <sup>+</sup> (mg/L)	4.12E+02	2.97E+02	2.94E+02	2.82E+02
Mg <sup>2+</sup> (mg/L)	8.14E+02	8.35E+02	8.52E+02	8.42E+02
Ca <sup>2+</sup> (mg/L)	2.09E+03	2.06E+03	2.13E+03	2.09E+03
Sr <sup>2+</sup> (mg/L)	4.79E+01	4.76E+01	4.88E+01	4.89E+01
Mn <sup>2+</sup> (mg/L)	1.40E+00	1.40E+00	1.40E+00	1.40E+00
Fe <sub>tot</sub> (mg/L)	7.40E+00	6.70E+00	6.40E+00	5.56E+00
Cl <sup>-</sup> (mg/L)	1.34E+05	1.39E+05	1.36E+05	1.39E+05
SO <sub>4</sub> <sup>2-</sup> (mg/L)	3.89E+03	3.68E+03	3.64E+03	3.74E+03
HCO <sub>3</sub> <sup>-</sup> (mg/L)	8.80E+01	5.70E+01	5.60E+01	5.87E+01
TDS (mg/L)	2.29E+05	2.36E+05	2.31E+05	2.36E+05

**Table 3** Post-injection fluid composition (PI) produced during back-production experiment from the injection/observation well Ktzi 201

Parameter	PI-1	PI-2	PI-3	PI-4	PI-5	PI-6	PI-7	PI-8	PI-9	PI-10
Date	16.10.2014	16.10.2014	17.10.2014	18.10.2014	19.10.2014	20.10.2014	21.10.2014	23.10.2014	26.10.2014	27.10.2014
pH	6.00	6.13	6.20	6.22	6.14	6.20	6.25	6.21	6.17	6.23
Na <sup>+</sup> (mg/L)	8.51E+04	8.53E+04	8.55E+04	8.63E+04	8.51E+04	8.55E+04	8.60E+04	8.62E+04	8.46E+04	8.55E+04
K <sup>+</sup> (mg/L)	8.34E+02	8.45E+02	8.32E+02	8.33E+02	8.30E+02	8.33E+02	8.33E+02	8.55E+02	8.96E+02	8.69E+02
Mg <sup>2+</sup> (mg/L)	9.51E+02	9.40E+02	9.46E+02	9.33E+02	9.44E+02	9.46E+02	9.45E+02	9.37E+02	9.44E+02	9.53E+02
Ca <sup>2+</sup> (mg/L)	2.04E+03	2.02E+03	2.03E+03	2.03E+03	2.06E+03	2.03E+03	2.03E+03	2.04E+03	2.05E+03	2.06E+03
Sr <sup>2+</sup> (mg/L)	5.20E+01	5.10E+01	5.10E+01	5.10E+01	5.10E+01	5.10E+01	5.10E+01	5.10E+01	5.00E+01	5.00E+01
Mn <sup>2+</sup> (mg/L)	2.39E+00	2.35E+00	1.47E+00	1.39E+00	1.84E+00	1.70E+00	1.81E+00	1.92E+00	1.86E+00	2.30E+00
Fe <sub>tot</sub> (mg/L)	3.71E+02	3.39E+02	3.43E+02	3.05E+02	3.00E+02	3.11E+02	2.99E+02	3.03E+02	3.01E+02	3.07E+02
Cl <sup>-</sup> (mg/L)	1.41E+05	1.51E+05	1.38E+05	1.37E+05	1.35E+05	1.39E+05	1.39E+05	1.37E+05	1.38E+05	1.37E+05
SO <sub>4</sub> <sup>2-</sup> (mg/L)	4.42E+03	4.02E+03	4.08E+03	3.96E+03	3.94E+03	4.49E+03	4.20E+03	4.15E+03	4.15E+03	4.31E+03
HCO <sub>3</sub> <sup>-</sup> (mg/L)	2.42E+03	2.34E+03	2.28E+03	2.20E+03	2.40E+03	2.44E+03	2.39E+03	2.36E+03	2.21E+03	2.15E+03
TDS (mg/L)	2.38E+05	2.47E+05	2.34E+05	2.34E+05	2.31E+05	2.35E+05	2.36E+05	2.34E+05	2.33E+05	2.33E+05

integrity monitoring program (Schmidt-Hattenberger et al. 2018). The first video inspection was conducted in October 2009 and continued with a yearly interval until the down-hole cementation of the respective wells (Fig. 2). Due to the early well abandonment of Ktzi 202 (cemented downhole in 2013), the last video camera inspection of the reservoir was already in October 2012, while the video camera inspection of the other wells continued until the final abandonment by May 2017.

In October 2011, at the observation well Ktzi 202, colorless prismatic crystals were observed at the well perforation holes with an inward growing direction in a bottom filter screen at a depth of 650–651 m [Fig. 3(a)]. The filter screen provides a hydraulic connection to the reservoir. In the upper parts of the observation well (about down to ~400 m), gaseous and liquid CO<sub>2</sub> coexist, while below this depth, liquid CO<sub>2</sub> prevails (Henninges et al. 2011). The precipitation was observed in the single-phase CO<sub>2</sub>. In the other observation wells, no similar precipitation was observed.

The crystals were sampled in October 2012 using a catch-container underneath the camera (Pers. Comm. Fabian Möller (GFZ)). The sampled crystals were cleaned for about fifteen minutes in an ultrasonic bath with ultra-pure ethanol. The crystals were colorless and ranged in size from a few millimeters up to a maximum of two centimeters. They are characterized by a mostly flat-planar or rarely elongated-prismatic habit [Fig. 3(b)]. The cleavage is typically perfect; however, it sometimes also developed fibrous, so that some crystals showed large slip plates. A few crystals have grown slightly curved. The crystal samples were analyzed by X-ray diffractometry (XRD). The mineral phase content analysis showed that the crystals are pure gypsum (CaSO<sub>4</sub>\*2H<sub>2</sub>O) (Fig. 4). Based on the video camera inspection and XRD analysis, no indication of other mineral precipitation is found, and only gypsum precipitation was observed at the filter screen (anhydrite was not found).

## Modeling methods

### Program code and database

The geochemical code PHREEQC [version 3.4; Parkhurst and Appelo (2013)] was used to reproduce the observations of the field monitoring with theoretical modeling results. Pitzer database (*Pitzer.dat*, with keyword *PITZER*), which is provided with the code PHREEQC was applied due to the high ionic strength of the brine solutions. The solutions are highly saline with high CO<sub>2</sub> partial pressure for this work, with ionic strength in the range of 4.5–5.0 mol/kgw. In these cases, a proper calculation model is needed to account for the brine, such as the specific ion interaction model developed by Pitzer (1973). The Pitzer database can

**Fig. 2** Life cycle of the Ketzin CO<sub>2</sub> storage with the video camera inspection (month/year)

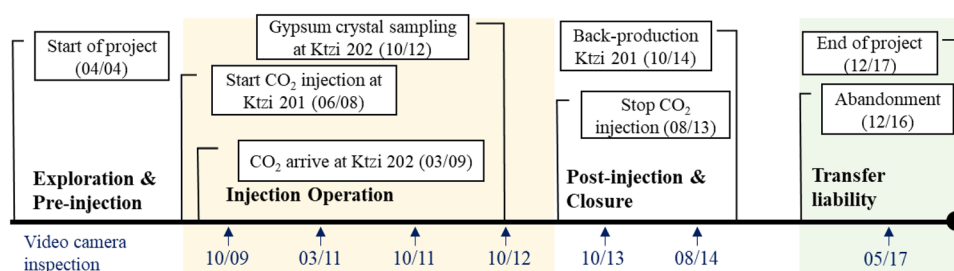


**Fig. 3** **a** Screenshot of the camera inspection of well Ktzi 202 in October 2011 at a depth of 650.6 m. The fibrous gypsum and gypsum needles in the well perforation holes grow roughly perpendicular to the wall. **b** Samples in the laboratory before and after ultrasonic cleaning (right and left, respectively). The samples are colorless to white and have a monoclinic crystal system

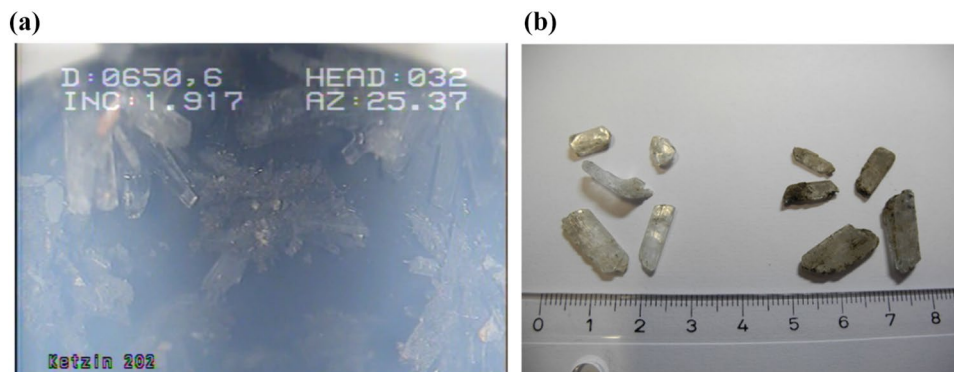
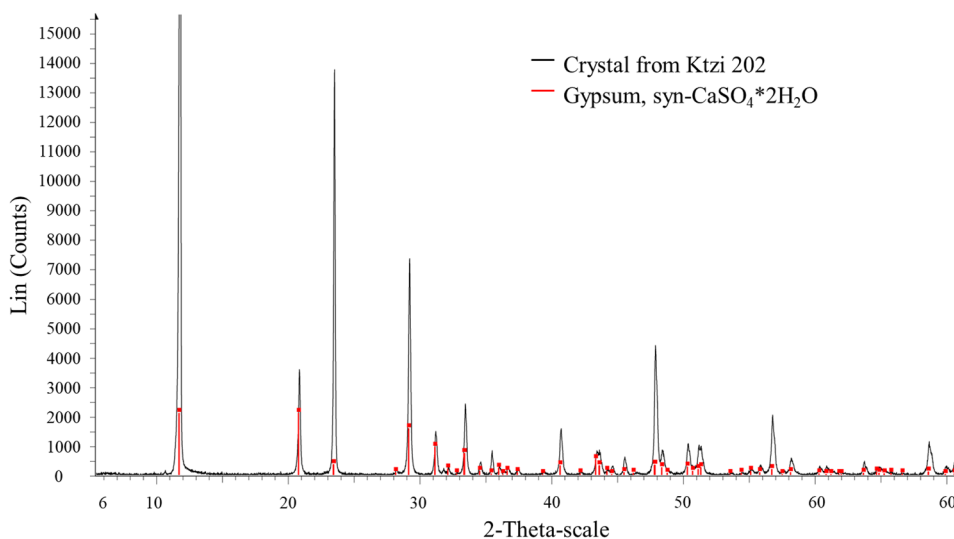


**Fig. 4** XRD diffractogram (peak position versus intensity) of the obtained crystals from Ktzi 202. The measured graph is the black line, the red peaks denote the peak positions for gypsum. The high similarity suggests that gypsum is the only mineral phase



cope with high-salinity waters that are beyond the range of the Debye-Hückel theory and calculate activity coefficients using Pitzer's ion interaction theory (Appelo et al. 2014). The Pitzer database, however, includes only a limited number of species. For example, aluminum (Al) is not available, which would be necessary for the calculation of the dissolution and precipitation of the present Al-containing minerals. Nevertheless, the Pitzer database defines the most consistent aqueous model that provides accurate mineral solubility prediction at high ionic strength (> 1.5 M) (Debure et al. 2019), particularly for the salinity of CO<sub>2</sub> storage conditions (Parkhurst and Appelo 2013; Tremosa et al. 2014). Some

mineral solubility predictions, in particular those related to the behavior of carbonates and calcium sulfates, are included in the database and, therefore, in the model.

### Geochemical reaction system

The CO<sub>2</sub>-brine-mineral interactions are analyzed with geochemical batch modeling. Four baseline (B) and ten post-injection (PI) brine solutions were sampled from the well Ktzi 202 and well Ktzi 201, respectively, and analyzed under surface conditions as listed in Tables 2 and 3. The averages

**Table 4** Mean geochemical values and standard deviations with changes between baseline (B) and Post-injection (PI) samples

Parameter	Baseline (B)		Post-injection (PI)		B to PI mean change (%)		
	Mean	SD ( $\sigma$ )	Mean	SD ( $\sigma$ )			
pH	6.53E+00	1.09E-01	6.18E+00	6.86E-02	- 5.30		
	(mg/L)	(mol/kg)	(mg/L)	(mol/kg)	(mol/kg)		
Na <sup>+</sup>	8.92E+04	4.23E+00	7.67E-02	8.55E+04	4.06E+00	2.95E-02	- 3.86
K <sup>+</sup>	3.21E+02	8.95E-03	1.44E-03	8.46E+02	2.36E-02	5.69E-04	164.10
Mg <sup>2+</sup>	8.36E+02	3.75E-02	6.96E-04	9.44E+02	4.24E-02	3.06E-04	13.21
Ca <sup>2+</sup>	2.09E+03	5.69E-02	6.30E-04	2.04E+03	5.55E-02	3.57E-04	- 2.48
Sr <sup>2+</sup>	4.83E+01	6.01E-04	7.48E-06	5.09E+01	6.35E-04	8.07E-06	5.64
Mn <sup>2+</sup>	1.40E+00	2.78E-05	9.98E-08	1.90E+00	3.78E-05	6.70E-06	36.24
Fe <sub>tot</sub>	6.52E+00	1.27E-04	1.26E-05	3.18E+02	6.22E-03	4.72E-04	4793.34
Cl <sup>-</sup>	1.37E+05	4.21E+00	8.03E-02	1.39E+05	4.29E+00	1.51E-01	1.89
SO <sub>4</sub> <sup>2-</sup>	3.74E+03	4.24E-02	1.03E-03	4.17E+03	4.75E-02	2.02E-03	11.93
HCO <sub>3</sub> <sup>-</sup>	6.49E+01	1.14E-03	2.27E-04	2.32E+03	4.13E-02	1.81E-03	3511.86
TDS	2.33E+05	8.58E+00	1.55E-01	2.35E+05	8.57E+00	1.68E-01	- 0.16

of the B and PI solutions, summarized in Table 4, are used to model the CO<sub>2</sub>-brine-mineral interactions.

The mineral phases have a fast reaction compared to the relevant timescales of several years, wherefore geochemical equilibrium is appropriate to be assumed. The precipitation and dissolution of the minerals are calculated using a mass-action equation at local equilibrium. The saturation index of gypsum, for example, is defined as follows (Eq. (1))

$$SI_{\text{gypsum}} = \log_{10} \left( \frac{\gamma_{Ca}[Ca]\gamma_{SO_4}[SO_4](a_{H_2O})^2}{K_{sp, CaSO_4 \times 2H_2O}} \right), \quad (1)$$

where  $[i]$  and  $\gamma$  are the solubility (in molality) and activity coefficients of species  $i$ , and  $K_{sp}$  is the solubility product. Accordingly,  $SI > 0$  implies a supersaturated solution, whereas  $SI < 0$  is an undersaturated solution.  $SI$  should be zero when solids are at equilibrium with the solution. The temperature- and pressure-dependent volume of aqueous species are calculated with a Redlich-type equation, and the CO<sub>2</sub> solubility is calculated by a Peng-Robinson model. A detailed description of the equations implemented to the PHREEQC code and CO<sub>2</sub>-water reaction calculation can be found in Appelo et al. (2014).

Table 5 summarizes the mineral dissolution and precipitation reactions considered in the simulation. The considered mineral phases are anhydrite, gypsum, dolomite, calcite, magnesite, and halite. The calcium sulfate minerals, anhydrite and gypsum, are present as the cement for the sandstone. Dolomite has been selected since dolomite is present as a pore-filling cement phase with the calcium sulfate minerals. Calcite, magnesite, and halite are included as secondary mineral phases. CaCO<sub>3</sub> precipitates only in calcite with

**Table 5** Mineral phases and reactions considered in the simulation

Mineral phase	Dissolution/precipitation reaction	LogK at 25 °C, 1 bar
Anhydrite	CaSO <sub>4</sub> ↔ Ca <sup>2+</sup> + SO <sub>4</sub> <sup>2-</sup>	- 4.25
Calcite	CaCO <sub>3</sub> ↔ Ca <sup>2+</sup> + CO <sub>3</sub> <sup>2-</sup>	- 8.50
Dolomite	CaMg(CO <sub>3</sub> ) <sub>2</sub> ↔ Ca <sup>2+</sup> + Mg <sup>2+</sup> + CO <sub>3</sub> <sup>2-</sup>	- 17.08
Gypsum	CaSO <sub>4</sub> × 2H <sub>2</sub> O ↔ Ca <sup>2+</sup> + SO <sub>4</sub> <sup>2-</sup> + 2H <sub>2</sub> O	- 4.60
Halite	NaCl ↔ Na <sup>+</sup> + Cl <sup>-</sup>	1.58
Magnesite	MgCO <sub>3</sub> ↔ Mg <sup>2+</sup> + CO <sub>3</sub> <sup>2-</sup>	- 7.83

All calculations were performed at thermodynamic equilibrium

no aragonite for modeling. The secondary mineral phases are introduced into the model as mineral phases are allowed to precipitate as a result of high CO<sub>2</sub> injection and the dissolution of primary minerals. In order to be able to handle the very complex natural composition of the reservoir sandstone numerically, the number of the considered minerals in the model was reduced. Some primary minerals were excluded from the model. Biotite, for example, is excluded due to its low concentration. Quartz is considered inert and, thus, excluded from modeling despite the significant portion in the Stuttgart Formation since quartz sandstones are usually expected to be geochemically stable (Labus and Wertz 2017). Potassium feldspar (K-feldspar) contains silicon, aluminum, and other elements are not present in the Pitzer Database. Therefore, silicate mineral reactions, as well as the behavior of clay minerals, cannot be addressed here. Moreover, in the present study, the special consideration is set to the calcium sulfate minerals based on the field observation. Thus, the silicate mineral reactions are not considered for the

modeling, unlikely to contribute significantly to the gypsum precipitation under saline conditions, although they are reservoir rock-forming minerals at the Ketzin site.

### Geochemical modeling approach

The modeling workflow consists of the following four steps. The first and second steps analyze the baseline and the impact of CO<sub>2</sub> injection at the reservoir conditions, respectively. The third step is a sensitivity analysis, with Step 4 as a final step calculating the amount of gypsum precipitation at the Ketzin. The corresponding geochemical solutions are listed in Table 6.

#### Step 1: analysis of reservoir conditions

The baseline (B) and post-injection (PI) chemical equilibria are analyzed. The B-S and PI-S solutions (Table 6) were analyzed under surface conditions. First, the chemical composition of the brine samples is recalculated to reservoir conditions, B-R and PI-R, respectively. The baseline reservoir condition is set as 34.5 °C and 63.5 bar, and the post-injection reservoir condition is defined as the same temperature and a pressure of 65.5 bar. The inorganic carbon is treated differently. For the baseline, the amount of the analyzed inorganic carbon is maintained between surface and reservoir conditions. For the post-injection, the solution is

equilibrated with the CO<sub>2</sub> partial pressure of 63.5 bar. The aqueous solution speciation calculation is conducted, and the mineral saturation indices are calculated.

The baseline and post-injection reservoir solutions (B-R and PI-R) are equilibrated with different scenarios of mineral phases, as listed in Table 7. The aim is to analyze the potential mineral dissolution of precipitation reaction paths and draw conclusions about the existence of minerals phases in the reservoir.

#### Step 2: CO<sub>2</sub> injection

This step calculates the geochemical and mineralogical changes due to the CO<sub>2</sub> injection. Based on the B-RMx solution, the CO<sub>2</sub> injection is carried out by numerically increasing CO<sub>2</sub> partial pressure to the post-injection reservoir conditions (referred to as B-RMx-CO<sub>2</sub>). For modeling, it is assumed that the CO<sub>2</sub> partial pressure is identical to the observed reservoir pressure, and the dissolved CO<sub>2</sub> is assumed in equilibrium with a constant pressure of the CO<sub>2</sub> gas phase.

Mineral changes and effects on pH are analyzed. The saturation indices indicate chemically active mineral phases. The resulting B-RMx-CO<sub>2</sub> solution is compared to the post-injection brine PI-R solution. Ideally, both brine solutions would be identical. The B-RMx-CO<sub>2</sub> and PI-R solutions are

**Table 6** Summary of brine solutions used in this study

Brine solution	Modeling Step	Description
B-S	Step 1	Baseline at surface conditions
B-R	Step 1	Baseline at reservoir conditions
PI-S	Step 1	Post-injection at surface conditions
PI-R	Step 1	Post-injection at reservoir conditions
B-RMx	Step 1	B-R equilibrated with reservoir minerals
PI-RMx	Step 1	PI-R equilibrated with reservoir minerals
B-RMx-CO <sub>2</sub>	Step 2	B-RM with equilibrated with reservoir minerals and CO <sub>2</sub>
B-CO <sub>2</sub>	Step 3	B-RM2-CO <sub>2</sub> for sensitivity analysis (reference model)
B-CO <sub>2</sub> -Ktzi	Step 4	B-RM2-CO <sub>2</sub> for the Ketzin

*B* refers to baseline, *PI* to post-injection, *S* refers to surface and *R* to reservoir conditions, *RM* additionally in equilibrium with different minerals. The *x* is a placeholder for the scenarios each representing a specific mineral combinations, as specified in Table 7.

**Table 7** Summary of the equilibrium model analysis scenarios

Solution	RM1	RM2	RM3	RM4	RM5	RM6	RM7
Primary minerals	Cal.			Cal.	Cal.		Cal.
		Dol.		Dol.		Dol.	Dol.
			Gyp.		Gyp.	Gyp.	Gyp.

The minerals selected for the primary mineral are calcite, dolomite, and gypsum. Note that magnesite and halite were arbitrarily added as potential secondary phases in all scenarios

*Cal.* calcite, *Dol.* dolomite, *Gyp.* gypsum



compared with respect to the changes in pH, major ions concentrations, and mineral phases.

**Step 3: sensitivity analysis**

The gypsum precipitation is calculated as a function of CO<sub>2</sub> concentration (CO<sub>2</sub> partial pressure of 20–100 bar), reservoir temperature (20–40 °C), and pressure (70–100 bar) to identify the changes in brine composition and the potential formation of the calcium sulfate minerals. The best matching model from the equilibrium analysis (Step 2) is chosen as the reference model (B-CO<sub>2</sub>). The results of the reference model serve as a basis for comparison with all other analyses.

It should be noted that the target reservoir temperature in this sensitivity analysis is within the Ketzin reservoir’s temperature range (about 20–40 °C). Calcium sulfate mineral solubility under different temperatures has been carried out by many researchers (Dai et al. 2017; Reiss et al. 2021) and found that for the relatively low-temperature range (up to a temperature of 40–60 °C), gypsum is the stable mineral phase (Dai et al. 2017; Van Driessche et al. 2019). Above this temperature range, anhydrite becomes the stable mineral phase (Reiss et al. 2021).

**Step 4: mineral precipitation at the Ketzin**

As the final step, the potential mineral precipitation related to the observed precipitated minerals in the observation well Ktzi 202 is discussed. Reservoir temperature and hydrostatic pressure at a depth of 650 m are varied for each period measured, and the imposed CO<sub>2</sub> concentration is assumed to be equal to the reservoir pressure.

**Geochemical modeling results**

**Geochemical interpretation**

The most apparent differences between B and PI samples are the concentration changes of bicarbonate (HCO<sub>3</sub><sup>-</sup>), iron (Fe<sub>tot</sub>), and potassium (K<sup>+</sup>) (see Table 4). The increase of bicarbonate is explained by CO<sub>2</sub> injection. Injected CO<sub>2</sub> dissolves in water and produces carbonic acid (H<sub>2</sub>CO<sub>3</sub>), then dissociation forming bicarbonate, which has an important impact on the subsequent geochemical reactions, that are analyzed in this paper. The increase of iron (Fe<sub>tot</sub>) concentration may have different reasons. Recent detailed mineralogical results show the presence of early diagenetic iron oxide coating in the baseline minerals (Förster et al. 2019). The dissolution of these under a CO<sub>2</sub>-induced acidic environment may appear reasonable. The Ketzin wells have an identical casing layout, including a stainless casing, which is subject to a specific dissolution reaction in the acidic environment,

contributing to increasing iron concentration in the PI samples. Kasina et al. (2017) hypothesized the leaching from silicate bound iron in reservoir rocks such as illite. However, the contribution to the iron may be small, considering that iron is only a minor component in the clay minerals and that the increase of iron is in the same order of magnitude as potassium (K<sup>+</sup>). The higher amount of potassium in the PI solution is explained by the dissolution of K-feldspar and illite, which are reservoir rock-forming minerals at the Ketzin site. The mean of the sodium (Na<sup>+</sup>) concentration decreases, which is an artifact, but this is caused by a problem of the analytical method, which is related to the high post-injection standard deviation. The concentrations of sulfate (SO<sub>4</sub><sup>2-</sup>) and magnesium (Mg<sup>2+</sup>) are slightly increased after the CO<sub>2</sub> injection. The increase of sulfate and magnesium concentration is hypothesized to originate from the local dissolution of anhydrite and dolomite, respectively (Förster et al. 2019). Especially the increase of sulfate is counter-intuitive to the precipitation of gypsum. A possible reason is a slightly different equilibrium due to the different sampling locations since the B and PI solutions are obtained from the well Ktzi 202 and well Ktzi 201, respectively. The increase is 5.10E-03 mol or remarkably almost 12%, which is nevertheless small considering the standard deviation of 2.02E-03 mol of the PI samples, wherefore it is plausible that the differences are based on the analytical limitations. The pH value is only slightly decreased in spite of the CO<sub>2</sub> injection, suggesting a pH-buffering reaction. The TDS content remains similar.

**Step 1: analysis of reservoir conditions**

The first step is to determine the baseline condition at the reservoir pressure and temperature. The pH value at baseline reservoir condition (B-R) is 6.46 and slightly lower than the pH value of 6.53 measured at the surface (B-S) due to an increase in temperature. The saturation indices are shown

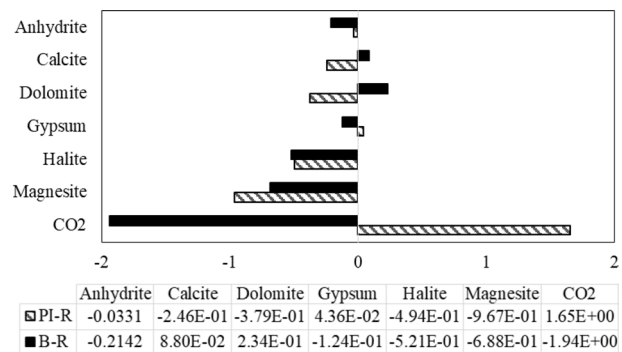


**Fig. 5** Mineral saturation index (SI) and CO<sub>2</sub> fugacity (log f<sub>CO<sub>2</sub>) calculations. B-R and PI-R are the recalculated B and PI solutions under the baseline and post-injection reservoir conditions, respectively</sub>

in Fig. 5. Anhydrite, calcite, dolomite, and gypsum are near saturation ( $|\log SI| < 0.5$ ), while halite and magnesite are clearly undersaturated in the B-R solution. Carbon dioxide fugacity ( $\log f_{\text{CO}_2}$ ) of  $-1.94$  is obtained. This value is in the range of typical  $\text{CO}_2$  in sedimentary formations for the corresponding temperature (Coudrain-Ribstein et al. 1998).

### Baseline scenarios

The baseline solution (B-R) is compared with different geochemical equilibrium scenarios, including various combinations of mineral assemblages shown in Table 7. Three metrics allow for comparing the baseline solution (B-R) with the scenario-based equilibrium solutions (B-RM1 to B-RM7). The equilibrium models analyze  $\text{CO}_2$ -independent reactions by equilibrating the mineral assemblage phases with the baseline solution. These are pH, the concentration of  $\text{Ca}^{2+}$ ,  $\text{Mg}^{2+}$ , and  $\text{SO}_4^{2-}$ , and mineral phases (Table 8). As the baseline solution (B-R) is close to equilibrium with respect to the carbonate minerals (see Fig. 5), the pH decreases only by about 0.1 units equilibration with calcite and dolomite. There is no difference between the pH-buffering capacity of dolomite and calcite. When the solutions are equilibrated with gypsum (B-RM3, 5, 6, and 7), the recalculated pH values are marginally low due to the dissolution of gypsum.

In all equilibrium scenarios, the dissolution of calcite and gypsum is observed, indicating that these mineral phases are unstable for the baseline solution. However, the baseline solution is only about 0.1 pH units above equilibrium. Considering the standard deviation of the pH values that are used to calculate the average pH is 0.1 (Table 4), it appears reasonable that the real pH is just slightly lower than the measured value, and the baseline solution is in equilibrium. Although calcite is oversaturated in the baseline solution, it is unstable after equilibration. Dolomite is more stable and preferably precipitates, leading to the dissolution of calcite.

More relevant differences can be found for  $\text{Ca}^{2+}$  and  $\text{SO}_4^{2-}$  concentrations. When gypsum and calcite are

considered as primary minerals (B-RM3, 5, 6, and 7),  $\text{Ca}^{2+}$  and  $\text{SO}_4^{2-}$  concentrations are higher than the B-R solution, about 14% and 19%, respectively. For all scenarios, where calcite is primary while gypsum is not (B-RM 1 and 4),  $\text{Mg}^{2+}$  concentration is about 10% lower than in the reservoir baseline. Dolomite precipitation brings to drop the concentration of  $\text{Ca}^{2+}$  and  $\text{Mg}^{2+}$ . However, the potential precipitation of dolomite does not significantly affect the  $\text{Ca}^{2+}$  and  $\text{Mg}^{2+}$  concentration as it precipitates only a minimal concentration. Overall, the concentration of the considered species in the reservoir could be best reproduced with the B-RM2 scenario solution, suggesting that only dolomite is reactive as a primary mineral phase.

### Post-injection scenarios

The recalculation of the brine composition to reservoir condition is also carried out for the post-injection solution (PI), with temperature, pressure, and  $\text{CO}_2$  partial pressure increased to the reservoir values. For the resulting PI-R solution, the pH value decreases from 6.18 to 4.45 (Table 9) due to the high  $\text{CO}_2$  partial pressure of 65.5 bar under the post-injection condition. The pH value of the measured PI solution is higher than that of the PI-R due to the  $\text{CO}_2$  degassing. During sampling,  $\text{CO}_2$  degassing occurs because of the pressure difference between reservoir depth and the earth's surface. The mineral saturation index (Fig. 5) shows that anhydrite and gypsum are still close to the equilibrium, but both saturation indices increase slightly compared to the baseline B-R. This could be a hint for the precipitation of calcium sulfate minerals. Calcite and dolomite change from slightly oversaturated pre-injection to slightly undersaturated post-injection condition. The decreasing carbonate saturation suggests that the carbonate minerals in the Stuttgart formation could be dissolved due to the  $\text{CO}_2$  injection.

The mineral equilibrium scenarios about the presence of primary minerals (listed in Table 7) are also tested for the PI solution (Table 9). Gypsum precipitates in all scenarios.

**Table 8** Selected parameters of the baseline reservoir brine for different scenarios of mineral equilibration

Brine solution	pH	Concentration (mol/kg)					
		$\text{Ca}^{2+}$	$\text{Mg}^{2+}$	$\text{SO}_4^{2-}$	$\Delta\text{Cal}$	$\Delta\text{Dol}$	$\Delta\text{Gyp}$
B-R	6.46	5.69E-02	3.75E-02	4.24E-02	–	–	–
B-RM1	6.37	5.99E-02	3.45E-02	4.24E-02	– 5.91E-03	2.97E-03	0.00E+00
B-RM2	6.37	5.69E-02	3.75E-02	4.24E-02	0.00E+00	1.41E-05	0.00E+00
B-RM3	6.34	6.49E-02	3.74E-02	5.04E-02	0.00E+00	1.78E-05	– 8.05E-03
B-RM4	6.37	5.99E-02	3.45E-02	4.24E-02	– 5.91E-03	2.97E-03	0.00E+00
B-RM5	6.34	6.51E-02	3.72E-02	5.03E-02	– 4.83E-04	2.59E-04	– 7.94E-03
B-RM6	6.34	6.49E-02	3.74E-02	5.04E-02	0.00E+00	1.78E-05	– 8.05E-03
B-RM7	6.34	6.51E-02	3.72E-02	5.03E-02	– 4.83E-04	2.59E-04	– 7.94E-03

The rows refer to different scenarios of primary mineral presented in the reservoir.  $\Delta$ Mineral refers to the mineral phase changes (mol/kg)

**Table 9** Selected parameters of the post-injection reservoir brine equilibrated with gypsum, dolomite, and calcite

Brine solution	pH	Concentration (mol/kg)					
		Ca <sup>2+</sup>	Mg <sup>2+</sup>	SO <sub>4</sub> <sup>2-</sup>	ΔCal	ΔDol	ΔGyp
PI-R	4.45	5.55E-02	4.24E-02	4.75E-02			
PI-RM1	4.55	5.96E-02	3.58E-02	3.94E-02	- 1.87E-02	6.64E-03	8.04E-03
PI-RM2	4.54	5.40E-02	4.48E-02	4.35E-02	0.00E+00	- 2.41E-03	3.92E-03
PI-RM3	4.45	5.29E-02	4.24E-02	4.48E-02	0.00E+00	0.00E+00	2.69E-03
PI-RM4	4.55	5.96E-02	3.58E-02	3.94E-02	- 1.87E-02	6.64E-03	8.04E-03
PI-RM5	4.55	5.96E-02	3.58E-02	3.94E-02	- 1.87E-02	6.64E-03	8.04E-03
PI-RM6	4.54	5.40E-02	4.48E-02	4.35E-02	0.00E+00	- 2.41E-03	3.92E-03
PI-RM7	4.55	5.96E-02	3.58E-02	3.94E-02	- 1.87E-02	6.64E-03	8.04E-03

The rows refer to different scenarios of primary mineral present in the reservoir. Gypsum precipitates in all scenarios. ΔMineral refers to the mineral phase changes (mol/kg)

Calcite dissolves when it presents as a primary mineral phase. Due to the changed geochemical equilibria, three different types can be distinguished. Type-1 shows identical results for PI-RM1, 4, 5, and 7, Type-2 offers identical results for PI-RM2 and 6, and Type-3 for PI-RM3. Type-1 is characterized by calcite dissolution that induces the gypsum and dolomite precipitation, releasing Ca<sup>2+</sup> ions into the solution, while Mg<sup>2+</sup> concentrations are too low compared with the PI-R solution. Type-2 includes dolomite buffering, resulting in a realistic Ca<sup>2+</sup> value, however, Mg<sup>2+</sup> is higher than measured (PI-R). Type-3 shows a slightly lower Ca<sup>2+</sup> value but fits for Mg<sup>2+</sup>. Additionally, the pH of Type-3 is best matched to the measured PI-R. Therefore, Type-2 and Type-3 are considered realistic for the post-injection conditions, with a slight preference for Type-3 (PI-RM3).

However, a perfect fit of the reality and model would find a scenario with identical composition to PI-R. Considering the sulfate concentration of Type-2 and Type-3, its value is about 4.00E-3 to 2.70E-3 mol/kg lower than the measured value PI-R. At the same time, Ca<sup>2+</sup> concentration is about 2 to 3\*E-03 mol/kg lower than the measured value and 3 to 4\*E-03 mol/kg gypsum precipitation. This may indicate that the reservoir brine is not in equilibrium but remains slightly oversaturated with respect to gypsum. The reason may be that the Pitzer database does not include the aqueous

neutral species CaSO<sub>4(aq)</sub>. The ions bond in this species do not contribute to the mass-action law but appear to be ions in chemical analysis. Unfortunately, the amount of the aqueous neutral species cannot be quantified, but it only can be expected that the ratio of neutral aqueous species is lower in high than in low salinity environments. Alternatively, it suggests that either measurement errors or inaccuracies in the geochemical model predict oversaturation of gypsum while it is very close to saturation.

### Step 2: synthetic CO<sub>2</sub> injection

In this step, the geochemical and mineralogical changes of the system due to the CO<sub>2</sub> injection are analyzed. CO<sub>2</sub> is introduced to the B-RM solution, and the synthetic output solution is referred to as B-RM-CO<sub>2</sub>.

A comparison between the baseline solutions with the simulated CO<sub>2</sub> injection (B-RMx-CO<sub>2</sub>) and the sampled post-injection solution (PI-R) is shown in Table 10. Ideally, one B-RMx-CO<sub>2</sub> scenario should reproduce the PI-R solution composition. The calculated pH values clearly show that the reservoir is buffered when the carbonate minerals are present, and the calculated pH values are similar to that of the calculated PI-R. With any carbonate mineral phases as the primary mineral phases, the calculated pH values are

**Table 10** Comparison of the sampled post-injection reservoir brine (PI-R) to the baseline brine solutions with modeled CO<sub>2</sub> injection (B-RMx-CO<sub>2</sub>) in the presence of the different primary mineral phases

Brine solution	pH	Concentration (mol/kg)					
		Ca <sup>2+</sup>	Mg <sup>2+</sup>	SO <sub>4</sub> <sup>2-</sup>	ΔCal	ΔDol	ΔGyp
PI-R	4.45	5.55E-02	4.24E-02	4.75E-02			
B-RM1-CO <sub>2</sub>	4.52	7.31E-02	3.75E-02	3.46E-02	- 2.40E-02	0.00E+00	7.79E-03
B-RM2-CO <sub>2</sub>	4.52	6.54E-02	4.96E-02	3.87E-02	0.00E+00	- 1.21E-02	3.73E-03
B-RM3-CO <sub>2</sub>	3.02	5.88E-02	3.75E-02	4.43E-02	0.00E+00	0.00E+00	- 1.90E-03
B-RM4-CO <sub>2</sub>	4.52	7.00E-02	4.27E-02	3.61E-02	- 1.41E-02	- 5.24E-03	6.30E-03
B-RM5-CO <sub>2</sub>	4.52	7.31E-02	3.75E-02	3.46E-02	- 2.40E-02	0.00E+00	7.79E-03
B-RM6-CO <sub>2</sub>	4.52	6.54E-02	4.96E-02	3.87E-02	0.00E+00	- 1.21E-02	3.73E-03
B-RM7-CO <sub>2</sub>	4.52	7.00E-02	4.27E-02	3.61E-02	- 1.41E-02	- 5.24E-03	6.30E-03

slightly higher than the PI-R solution and realistic, only about 0.1 units higher than the PI-R solution. Calcite only buffered (B-RM1-CO<sub>2</sub>) shows considerably high Ca<sup>2+</sup> and very low SO<sub>4</sub><sup>2-</sup> concentration, and dolomite only (B-RM2-CO<sub>2</sub>) shows a closer fit for Ca<sup>2+</sup> and SO<sub>4</sub><sup>2-</sup>, but Mg<sup>2+</sup> is too high with a similar difference as it was too low for calcite only scenario. Both calcite and dolomite buffered (B-RM4-CO<sub>2</sub>) shows the concentrations of the ions are between the single mineral buffered one, with the best results for Mg<sup>2+</sup> but worse for Ca<sup>2+</sup> and SO<sub>4</sub><sup>2-</sup>. The B-RM3-CO<sub>2</sub> scenario provides the best fit for Ca<sup>2+</sup> and SO<sub>4</sub><sup>2-</sup> concentrations with substantially low pH. Considering the ion's concentration and the calculated pH value, dolomite only (B-RM2-CO<sub>2</sub>) or mixed buffered scenario (B-RM6-CO<sub>2</sub>) appear most approvable.

Gypsum precipitation is similar for the calcite only (B-RM1-CO<sub>2</sub>) and calcite together with gypsum (B-RM5-CO<sub>2</sub>), and considerably low for the dolomite scenario (B-RM2-CO<sub>2</sub>). This occurs as the dissolution of carbonates releases Ca<sup>2+</sup> ions that lead to calcium sulfate precipitation. Similar CO<sub>2</sub>-induced mineral alteration experiments have been conducted with the experimental evidence by Garcia-Rios et al. (2014). They set up a flow-through experimental system that allows exploring the interaction between CO<sub>2</sub>-rich sulfate solutions and carbonate reservoir rocks and demonstrated that the dissolution of carbonate minerals and the precipitation of gypsum. However, gypsum would dissolve when gypsum presents as the only primary mineral and gives decrease the pH, similar to B-RM3-CO<sub>2</sub>. However, there is a mismatch between simulated and observed ion concentrations. Generally, SO<sub>4</sub><sup>2-</sup> concentration in all scenarios with CO<sub>2</sub> injection is comparatively low, even when no gypsum would precipitate. Ca<sup>2+</sup> concentrations are consistently too high compared to the field measurement (PI-R). The reason possibly, that the baseline samples were retrieved from the observation well 202, and the post-injection samples were retrieved from the injection well Ktzi 201.

### Synthesis of equilibrium models

Three fluid types were equilibrated, the baseline fluid (B), the post-injection fluid (PI), and the baseline fluid with simulated CO<sub>2</sub> injection (B-RMx-CO<sub>2</sub>). Each fluid was equilibrated with seven scenarios of the primary reservoir minerals.

The results of the different models allow concluding the geochemical conditions in the reservoir. The reservoir is clearly carbonate buffered. The main buffering system is done by dolomite. Simulations suggest that calcite was present at the baseline conditions and took part in the buffering, but under fully established CO<sub>2</sub> storage conditions, only dolomite appears to be the active primary mineral. Simulation results suggest that the gypsum is not a primary

mineral for the baseline conditions; however, it is simulated to precipitate all realistic scenarios. Therefore, the scenario B-RM2-CO<sub>2</sub>, where only dolomite presents as a primary mineral, is considered the most likely and therefore used in the sensitivity analysis.

### Step 3: sensitivity analysis

#### Reference model

The B-RM2-CO<sub>2</sub> model with dolomite as the primary mineral phase serves as a reference model to elucidate the effect of reservoir condition changes. With the imposed CO<sub>2</sub> partial pressure of 65.5 bar, the pH value of 4.52 is obtained.

#### Reservoir temperature and hydrostatic pressure

The impacts of the reservoir temperature and hydrostatic pressure on the gypsum precipitation are investigated. Except for each variable (temperature and pressure), other input parameters are maintained as the reference model B-RM2-CO<sub>2</sub>.

The simulation results show decreasing gypsum precipitation with increasing temperature [Fig. 6(a)]. The maximum gypsum precipitation occurs at the lowest temperature (20 °C, 6.06E-03 mol/kg), which is about 60% higher than the reference model. Within the temperature range from 20 to 40 °C, gypsum precipitation, the pH value at the lowest temperature shows that the highest pH value of 4.59, and the calculated pH value slightly decrease with the increasing temperature. Under the reservoir temperature of 40 °C, a pH value of 4.50 is obtained.

Gypsum precipitation decreases as the reservoir hydrostatic pressure increases, e.g., the precipitation decreases by 20% from 65.5 bar of the reference model to 100 bar (2.96E-03 mol/kg), resulting in increasing SO<sub>4</sub><sup>2-</sup> concentration [Fig. 6(b)]. That means increasing the reservoir pressure slightly reduces the gypsum precipitation under the constant CO<sub>2</sub> presence conditions. The calculated pH values were kept at around 4.52 within the pressure range of 65.5–100 bar. Similarly, Li and Duan (2011) used a thermodynamic model and found that the increase of pressure increases the solubility of calcium sulfate minerals. The solubility of gypsum increases with pressure since the sum of the aqueous molar volumes of the solute species is smaller than the molar volume of the minerals and water (Appelo et al. 2014). Our simulation results are consistent with the theoretical predictions.

#### CO<sub>2</sub> concentration

In this step, the imposed CO<sub>2</sub> partial pressure is varied to identify the gypsum precipitation changes under the

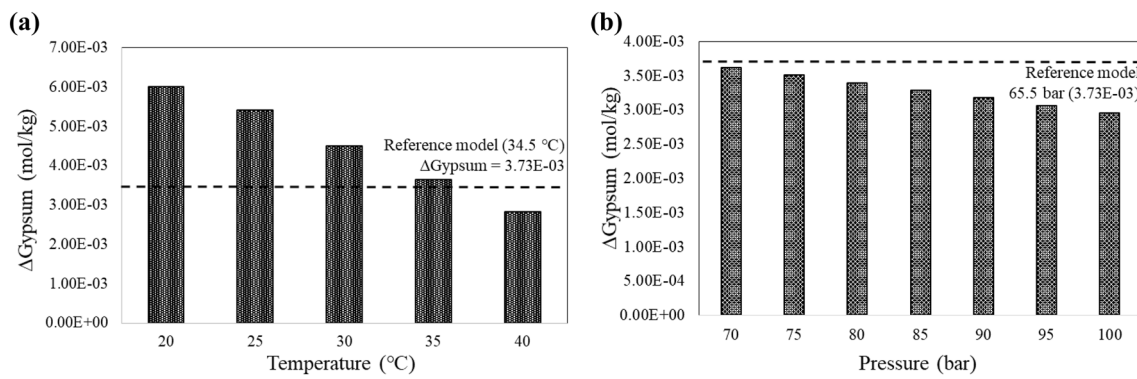


**Fig. 6** Gypsum precipitation with **a** the constant partial CO<sub>2</sub> pressure and hydrostatic pressure in temperatures ranging from 20 to 40 °C and **b** as a function of the reservoir pressure with the constant partial CO<sub>2</sub> pressure

reservoir condition, while temperature and pressure are maintained at their initial level. Again, except for the CO<sub>2</sub> concentration, other input parameters are the same as the reference model. To illustrate the impact, the CO<sub>2</sub> partial pressure exceeds the reservoir pressure, which is physically not possible in reality.

Based on this model, it can be seen that the gypsum precipitation increases as CO<sub>2</sub> concentration [Fig. 7(a)]. The gypsum precipitation with the CO<sub>2</sub> partial pressure of 100 bar (4.99E-03 mol/kg) is about two times larger than that of 50 bar (2.52E-03 mol/kg) and about 34% higher than the reference model (3.73E-03 mol/kg). Wolfe and Bennett (2011) proposed two potential factors for this behavior of gypsum precipitating as increasing CO<sub>2</sub> concentration. One of the factors is decreasing water activity due to the hydration of dissolved CO<sub>2</sub>. The decrease of water activity occurs by decreasing the availability of free water to maintain hydration of Ca<sup>2+</sup> and SO<sub>4</sub><sup>2-</sup> ions. Figure 7(b) shows that the water activity decreases as CO<sub>2</sub> concentration increases. The water activity with pCO<sub>2</sub> 100 bar is around 0.014 units lower than that of the pure brine solution. Here, the prediction by our modeling results shows a good agreement with

their experimental determination. The other factor is the destabilization of the calcium sulfate neutral species, such as CaSO<sub>4(aq)</sub>, due to the high concentration of CO<sub>2</sub> in the solution. The increasing dissolved CO<sub>2</sub> results in the increase of the destabilizing the neutral species CaSO<sub>4(aq)</sub> and drives precipitation of gypsum (Wolfe and Bennett 2011). Rendel et al. (2016) also observed a decreasing gypsum solubility with increasing CO<sub>2</sub> concentration by the laboratory experiments using a reaction pressure and temperature of 70 bar and 25 °C with varying CO<sub>2</sub> concentrations from 0 to 0.54 mol/kg. Our applied model is in agreement with the respective studies.

### Anhydrite–gypsum transition under CO<sub>2</sub> influence

The decrease in temperature favors the precipitation of sulfate minerals. The type of mineral precipitating changes with the temperature. Generally, Gypsum is stable below 40 °C, and anhydrite is stable above 130 °C. Between 40 and 130 °C, there is no clear identification of which is the stable phase (Dai et al. 2017).

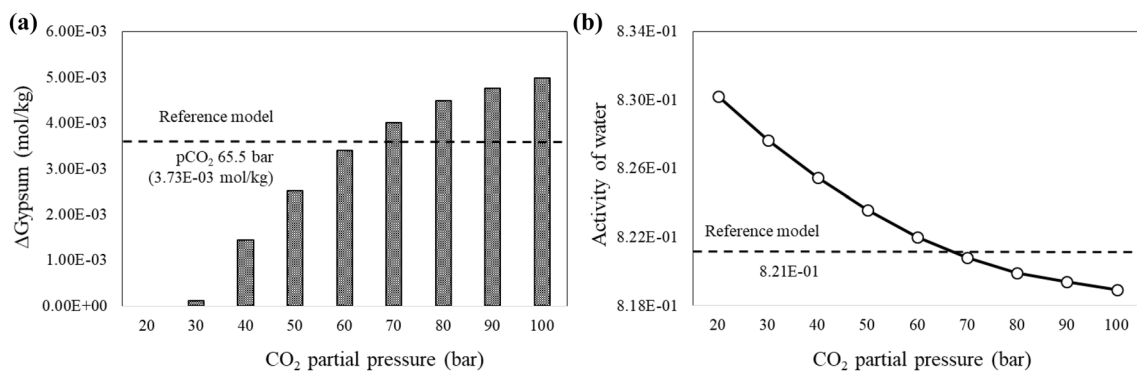


**Fig. 7** **a** Gypsum precipitation (mol/kg) and **b** changes of activity of water as a function of the imposed CO<sub>2</sub> partial pressure

In various CO<sub>2</sub> storage projects worldwide, the CO<sub>2</sub> is injected and stored at a deep reservoir with high pressure and temperature condition. For example, a massive amount of CO<sub>2</sub> injected was operated at a maximum depth of 1800 m at the Salah storage site in Algeria (Ringrose et al. 2013), and CO<sub>2</sub> was injected at about 2000 m depth at the Otway site in Australia (Underschultz et al. 2011). In the Lacq-Rousse pilot in France, the CO<sub>2</sub> injection was very deep at around 4500 m depth and performed in a depleted gas reservoir (Prinet et al. 2013). In these storage projects, a wide range of reservoir temperature and pressure conditions should be considered to avoid and predict the potential mineral precipitation. The geochemical modeling conducted in this work may help to predict geochemical effects during CO<sub>2</sub> storage operations and various p–T conditions. Calcium sulfate mineral precipitation is calculated at the different reservoir depths, with  $T (^{\circ}C) = 10 ^{\circ}C + \text{depth (m)} \times 3.75 ^{\circ}C/100 (m)$  and  $P (\text{bar}) = 11 \text{ bar}/100 (m) * \text{depth (m)}$ . The imposed CO<sub>2</sub> partial pressure is identical to the hydrostatic reservoir pressure (Fig. 8).

Gypsum starts to precipitate as depth increases, and the highest gypsum precipitation occurs at around 500 m. Then, with increasing depth, gypsum precipitation decreases, and,

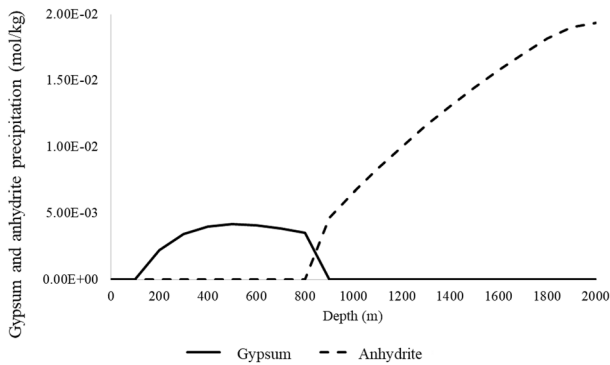


Fig. 8 Gypsum and anhydrite precipitation (mol/kg) with depth

at approximately 800 m, anhydrite starts to precipitate. Between 800 to 900 m, the gypsum-anhydrite transition is observed. The simulation results indicate that the calcium sulfate mineral precipitation should be carefully monitored, especially in high sulfate-rich brine solution throughout the depth. The effect could be relatively minor in the shallow depth; however, in the deeper reservoir, calcium sulfate mineral precipitation may significantly influence the local geochemical and geophysical systems since it may induce the well-logging and change of physicochemical characteristics.

#### Step 4: gypsum precipitation at Ktzi 202

The reference model (B-RM2-CO<sub>2</sub>) is applied to predict the gypsum precipitation for the Ketzin reservoir pressure and temperature conditions measured at the observation well Ktzi 202. The imposed CO<sub>2</sub> partial pressure is equal to the reservoir pressure for each period measured from March 2009 to October 2011.

As shown in Fig. 9, it can be expected that gypsum precipitates when the CO<sub>2</sub> arrives at the observation well, and the amount of precipitation gradually decreases until March 2010, mainly due to the increase in reservoir temperature. Then, the gypsum precipitation increases with the decrease in reservoir pressure and temperature. It should be noted that while gypsum precipitation increases with increasing CO<sub>2</sub> concentration, the effect of the CO<sub>2</sub> concentration on the gypsum precipitation is considerably smaller compared to that of the temperature and pressure in this model.

It should be emphasized that the temperature variations in the observation well are affected by CO<sub>2</sub> evaporation and condensation and also by well operations prior to the logging campaigns in which the p–T data are collected. The temperature variations, therefore, do not reflect the injection-related conditions in the reservoir. Nevertheless, the observed pressure in the well is identical to the reservoir pressure in close proximity to the well.

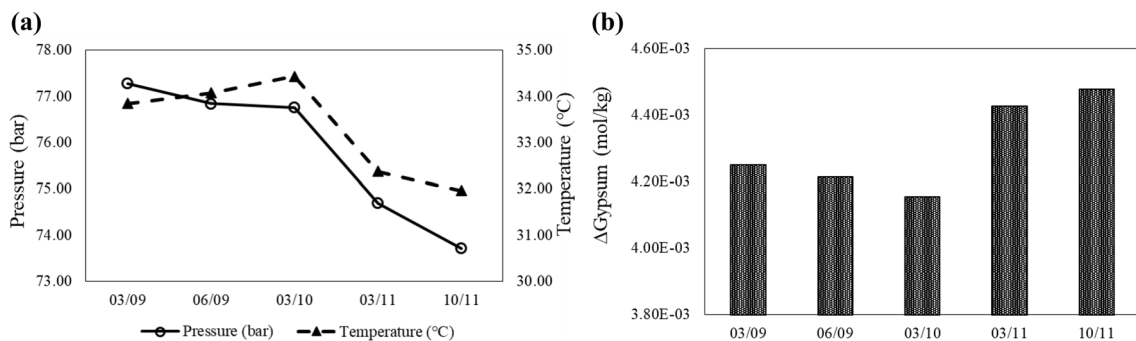


Fig. 9 a Reservoir pressure and temperature changes obtained from the observation well Ktzi 202 at a depth of 650 m and b gypsum precipitation prediction for selected months corresponding reservoir conditions (month/year)

## Discussion

After the CO<sub>2</sub> injection, colorless prismatic crystals were found at the inner surface of the filter screen at observation well Ktzi 202 at the Ketzin CO<sub>2</sub> storage site in Germany. Subsequent XRD analysis revealed that the crystals consist of single-phase pure gypsum; no anhydrite was found. The main goal of this study is to find out the mechanisms that lead to mineral precipitation.

The input data to the geochemical model are analyses of downhole fluid samples, baseline fluid samples (B) from the well Ktzi 202 prior to the CO<sub>2</sub> injection and post-injection (PI) samples from the well Ktzi 201 after the CO<sub>2</sub> injection. Mineralogical analyses of reservoir cores provide a geochemical context (Förster et al. 2019; Kasina et al. 2017; Norden and Frykman 2013). Some minerals may not be geochemically active due to, e.g., coatings, cement phases, or other reasons. The baseline conditions of the reservoir are modeled. Different scenarios are simulated to identify which minerals are in equilibrium with the reservoir brine. The resulting geochemical system is used to simulate the geochemical reactions induced by CO<sub>2</sub> injection.

A main difficulty to the geochemical modeling is the very high ionic strength of the reservoir brine of 4.5–5. This requires the Pitzer database to be used, although it has only a limited number of species. Therefore only gypsum, anhydrite, calcite, halite, and dolomite are included in the model. Other frequent reservoir minerals are feldspars and other silicates (Norden and Frykman 2013), which are not included in the Pitzer database. This limits the accuracy of the modeling. Nevertheless, feldspars and other silicates are expected to have orders of magnitude lower reactivity compared to sulfates and carbonates. The simulated equilibrium models and the changes due to the CO<sub>2</sub> injection suggest that the model allows for a reasonable interpretation of the field data. We interpret this as an indication that the present model covers the main geochemical processes.

The results for CO<sub>2</sub> injection clearly show that the pH is buffered. Dolomite is identified as the main buffer mineral for baseline and post-injection conditions. Under baseline conditions, maybe a certain amount of calcite was a chemically active buffer, but probably not during post-injection.

The model indicates that gypsum becomes oversaturated as a consequence of the CO<sub>2</sub> injection by two mechanisms. The first is that CO<sub>2</sub> dissociates and increases ionic strength, wherefore the activity of water is reduced, and saturation indices of all minerals are slightly increased. The second follows from the acid character of the solution. The results clearly show that the pH is buffered, primarily due to dolomite dissolution. During the reaction, calcium

ion is released into the solution. This shifts the equilibrium further to gypsum supersaturation. Both mechanisms require a baseline solution with gypsum close to saturation. Although gypsum is close to saturation, the baseline models indicate that gypsum is not a primary mineral in the reservoir.

The repeated pH measurements show a standard deviation of 0.1 pH units in the present study. The geochemical equilibrium for dolomite is also only 0.1 pH units away from the baseline composition. It appears reasonable that the determination accuracy of the pH may be the reason for the disequilibrium of the current model. Since the dolomite buffer reaction is considerably faster than the year scale of the injection, it is reasonable to assume that the reservoir brine is in equilibrium with dolomite under baseline conditions and in equilibrium with dolomite and gypsum for post-injection conditions. However, to some degree over- and under-saturations of minerals may also persist on longer time scales. Some gypsum might be present as a neutral aqueous species. In the geochemical analysis, this species appears as ions, but it does not contribute to the mass-action law. The Pitzer database does not provide this species, wherefore the model might overestimate the gypsum precipitation.

The highly saline environment is difficult to simulate. Mineral saturation calculations similar to this study have been carried out for the Ketzin brine solution using three different thermodynamic databases SCALE2000, SandiaLab, and Thermodem (Tremosa et al. 2014). They reported that calcite is slightly undersaturated with the Ketzin brine solution using these three databases. Interestingly, the saturation state of dolomite at the reservoir baseline condition is calculated differently; slightly oversaturated when using the SCALE2000 and SandiaLab databases, but undersaturated using the Thermodem database. Using the Pitzer database applied in this study, the modeling suggests that dolomite is slightly oversaturated for baseline with the brine solution and calcite as comparatively unstable. The difference in the saturation indices is related to the considerations of ion interaction of the different databases (Tremosa et al. 2014).

The brine samples analyzed in this study are from two different wells. This is certainly a potential error source, although the chemistry is very similar, and previous work indicates good hydraulic contact between the wells (Wagner and Wiese 2018; Wiese et al. 2010). A slight increase of the sulfate concentration is observed between baseline and post-injection and could be considered as a contraindication for gypsum precipitation. Förster et al. (2019) conjecture dissolution of sulfate as a reason for the slight increase. However, the increase of sulfate has a similar magnitude as the standard deviation of the sulfate concentrations of the individual baseline and post-injection samples, the slight increase is probably an artifact. Further, baseline samples are retrieved from the observation well Ktzi 202, while post-injection

samples were retrieved from the injection well Ktzi 201, which may be the reason for small variations in the composition. Our simulations indicate that gypsum is undersaturated under baseline reservoir conditions and that the presence of geochemically active gypsum would lead to unlikely high sulfate concentrations. Therefore, we consider the undersaturation for baseline conditions as rather unambiguous for gypsum, and calcium sulfate mineral dissolution after CO<sub>2</sub> injection is hence unlikely. As a logical consequence, we interpret the anhydrite, which is present partially in the reservoir, as not geochemically active on the reservoir scale. However, experiments with Ketzin cores in brine show that anhydrite can dissolve (Fischer et al. 2013).

The model appears to include the relevant chemical processes for the current timescale. In the longer-term than the considered interval of 6 years (time from injection starts until post-injection sampling during the back-production), the slower geochemical reactions of feldspars, clay minerals, and other silicates likely contribute to the geochemical equilibrium, wherefore the current model is not suitable for long-term predictions.

To investigate the responses to the interaction of CO<sub>2</sub>-charged brine with Ketzin reservoir sandstone, Förster et al. (2019) conducted core sample analysis from three drill campaigns; baseline core (Ktzi 200, 201, and 202) and after 4 years and 9 years of injection (Ktzi 201 and Ktzi 203, respectively). Although changes in mineralogy were minor, they found siderite and calcite. The authors argue that both minerals formed simultaneously due to the local dissolution of dolomite and anhydrite after the CO<sub>2</sub> injection. No post-injective calcium sulfate mineral precipitation was observed by the core rock analysis. These results are only for dolomite in accordance with predictions from our modeling. A possible reason is that the post-injection cores were retrieved with bentonite drilling mud, usually containing calcite, which was used during the side-track core experiment (Pers. Comm. UGS Mittenwalde). Another reason may be that some of the repeat samples were taken close to the injection well. As dry CO<sub>2</sub> is injected, a dry-out zone forms around the injection well. There, water evaporates to create a chemical milieu that is not representative of the reservoir and in which a series of minerals precipitates. No newly formed gypsum is found in post-injection rock core samples. A possible reason might be that gypsum dissolves easily, and especially small fresh crystals may be washed out during sample preparation, e.g., during cutting for thin-section preparation. And, as a typical impact, subsequent core analyses are carried out with different cores, wherefore spatial heterogeneity might mimic temporal variations.

The gypsum precipitation is only observed in the inner well-bore of Ktzi 202 during video camera inspection, but not in the other three reservoir penetrating wells. The gypsum crystals were observed first in October 2012, although

the geochemical model shows oversaturation of gypsum immediately after CO<sub>2</sub> arrival in the well in 2009. The pressure and temperature conditions for gypsum precipitation, nevertheless, were most favorable in October 2012. The reason for the lag in gypsum appearance remains unclear. Nevertheless, the newly formed gypsum crystals are clear evidence that the gypsum is formed to respond to interaction with the CO<sub>2</sub>-acidified brine and reservoir minerals.

At the Ketzin site, the amount (volume) of gypsum precipitates is rather small compared to the available pore volume of the reservoir and has only been observed in one observation well at Ketzin. Because neither gypsum precipitation nor other mineral precipitates at Ketzin in significant quantity have been reported yet, we argue that the observation of gypsum crystals in observation well Ktzi 202 does not hamper safe long-term CO<sub>2</sub> storage.

## Summery and conclusions

Two main results are presented within this work:

- Gypsum crystals have been found in observation well Ktzi 202 of the Ketzin reservoir.
- Post-injection brine samples have been analyzed within this work. They allow to identify the geochemical impact of CO<sub>2</sub> injection on the reservoir scale.

A rather simple geochemical model is set up using PHREEQC and the Pitzer database, allowing a reasonable representation of recent Ketzin baseline and post-injection fluid samples for Ca<sup>2+</sup>, Mg<sup>2+</sup>, SO<sub>4</sub><sup>2-</sup> and pH.

- For baseline conditions, the reservoir is considered in equilibrium with dolomite.
- The brine pH decreased after CO<sub>2</sub> injection and is buffered by dolomite dissolution, possibly with a minor contribution of calcite. For post-injection conditions, only the dolomite buffer remains.
- For baseline conditions, gypsum is undersaturated.
- Gypsum becomes oversaturated as a consequence of CO<sub>2</sub> injection.
- The oversaturation of gypsum occurs due to Ca<sup>2+</sup> release from dolomite dissolution and decreased water activity due to dissociation of CO<sub>2</sub> in the brine.
- Anhydrite is undersaturated for baseline and post-injection conditions.
- The calcium sulfate mineral precipitation potential increases by factor 5 from Ketzin pressure and temperature conditions at 640 m to typical CO<sub>2</sub> storage conditions in 2,000 m.
- Although the amount of potential calcium sulfate precipitation increases for deeper reservoirs, the specific



volume of anhydrite is lower than gypsum, wherefore, the clogging potential for deeper reservoirs is similar to the Ketzin conditions.

- An increased clogging hazard could exist if the pH-buffering reaction following CO<sub>2</sub> injection involves calcite instead of dolomite. In this case, more Ca<sup>2+</sup> ions would be released, resulting in a larger quantity of calcium sulfate precipitation. However, the geochemical conditions are highly site-specific, and individual storage sites have to be analyzed separately.

The presented study emphasizes the need to monitor baseline and post-injection conditions and to consider the potential formation of (calcium) sulfate minerals explicitly. Especially in the well-bore areas, unexpected consequences may occur and lead to clogging with the typical adverse consequences of the on-site operation, namely lowered injectivity.

More studies are needed before firm conclusions can be reached about the potential mineral precipitation due to CO<sub>2</sub> injection. The injection of CO<sub>2</sub> into the reservoir induces multi-phase flow and reactive mass transport processes that may significantly impact the spatial and temporal distribution of chemical components and mineral phases. Advanced computational simulation techniques are also required for further predicting both the short-term injection performance and the long-term trapping behavior of the CO<sub>2</sub> plume in future research.

**Funding** Open Access funding enabled and organized by Projekt DEAL. This paper is part of a project that has received funding by the European Union's Horizon 2020 research and innovation program under grant agreement no. ENER/H2020/764531/SECURE. Any opinions, findings and conclusions of recommendations expressed in this material are those of the authors and do not necessarily reflect the views of the European commission.

## Declarations

**Conflict of interest** There are no conflict of interest in this study.

**Open Access** This article is licensed under a Creative Commons Attribution 4.0 International License, which permits use, sharing, adaptation, distribution and reproduction in any medium or format, as long as you give appropriate credit to the original author(s) and the source, provide a link to the Creative Commons licence, and indicate if changes were made. The images or other third party material in this article are included in the article's Creative Commons licence, unless indicated otherwise in a credit line to the material. If material is not included in the article's Creative Commons licence and your intended use is not permitted by statutory regulation or exceeds the permitted use, you will need to obtain permission directly from the copyright holder. To view a copy of this licence, visit <http://creativecommons.org/licenses/by/4.0/>.

## References

- Appelo CAJ, Parkhurst DL, Post VEA (2014) Equations for calculating hydrogeochemical reactions of minerals and gases such as CO<sub>2</sub> at high pressures and temperatures. *Geochim Cosmochim Acta* 125:49–67
- Arslan A, Dutt G (1993) Solubility of gypsum and its prediction in aqueous-solutions of mixed electrolytes. *Soil Sci* 155:37–47
- Bacon DH, Sass BM, Bhargava M, Sminchak J, Gupta N (2009) Reactive transport modeling of CO<sub>2</sub> and SO<sub>2</sub> injection into deep saline formations and their effect on the hydraulic properties of host rocks. *Energy Procedia* 1(1):3283–3290
- Breen KJ, Angelo CG, Masters RW, Sedam AC (1985) Chemical and isotopic characteristics of brines from three oil- and gas-producing sandstones in eastern Ohio, with applications to the geochemical tracing of brine sources. *Geological Survey, US*, pp 84–4314. <https://doi.org/10.3133/wri844314>
- Coudrain-Ribstein A, Gouze P, de Marsily G (1998) Temperature-carbon dioxide partial pressure trends in confined aquifers. *Chem Geol* 145(1):73–89
- Dai Z, Kan AT, Shi W, Zhang N, Zhang F, Yan F, Bhandari N, Zhang Z, Liu Y, Ruan G, Tomson MB (2017) Solubility measurements and predictions of gypsum, anhydrite, and calcite over wide ranges of temperature, pressure, and ionic strength with mixed electrolytes. *Rock Mech Rock Eng* 50(2):327–339
- De Lucia M, Bauer S, Beyer C, Kühn M, Nowak T, Pudlo D, Reitenbach V, Stadler S (2012) Modelling CO<sub>2</sub>-induced fluid–rock interactions in the Altensalzwedel gas reservoir. Part I: from experimental data to a reference geochemical model. *Environ Earth Sci* 67(2):563–572
- Debure M, Lassin A, Marty NC, Claret F, Virgone A, Calassou S, Gaucher EC (2019) Thermodynamic evidence of giant salt deposit formation by serpentinization: an alternative mechanism to solar evaporation. *Sci Rep* 9(1):11720
- Emberley S, Hutcheon I, Shevalier M, Durocher K, Gunter WD, Perkins EH (2004) Geochemical monitoring of fluid-rock interaction and CO<sub>2</sub> storage at the Weyburn CO<sub>2</sub>-injection enhanced oil recovery site Saskatchewan, Canada. *Energy* 29(9):1393–1401
- Fischer S, Liebscher A, De Lucia M, Hecht L (2013) Reactivity of sandstone and siltstone samples from the Ketzin pilot CO<sub>2</sub> storage site-laboratory experiments and reactive geochemical modeling. *Environ Earth Sci* 70:3687–3708
- Förster HJ, Wilke F, Bock S, Eisner D, Förster A, Norden B, Schmidt-Hattenberger C (2019) Mineralogical responses to 9-years of interaction of a CO<sub>2</sub>-charged brine with a sandstone aquifer: observations and implications from the Ketzin CO<sub>2</sub>-storage pilot site (Germany), 10th International Trondheim CCS Conference: Trondheim, Norway p. 134
- Garcia-Rios M, Cama J, Luquot L, Soler JM (2014) Interaction between CO<sub>2</sub>-rich sulfate solutions and carbonate reservoir rocks from atmospheric to supercritical CO<sub>2</sub> conditions: experiments and modeling. *Chem Geol* 383:107–122
- Garcia-Rios M, Luquot L, Soler JM, Cama J (2015) Influence of the flow rate on dissolution and precipitation features during percolation of CO<sub>2</sub>-rich sulfate solutions through fractured limestone samples. *Chem Geol* 414:95–108
- Gaus I, Azaroual M, Czernichowski-Lauriol I (2005) Reactive transport modelling of the impact of CO<sub>2</sub> injection on the clayey cap rock at Sleipner (North Sea). *Chem Geol* 217(3):319–337
- Hennings J, Liebscher A, Bannach A, Brandt W, Hurter S, Köhler S, Möller F (2011) P-T-ρ and two-phase fluid conditions with inverted density profile in observation wells at the CO<sub>2</sub> storage site at Ketzin (Germany). *Energy Procedia* 4:6085–6090

- Kasina M, Bock S, Würdemann H, Pudlo D, Picard A, Lichtschlag A, März C, Wagenknecht L, Wehrmann LM, Vogt C, Meister P (2017) Mineralogical and geochemical analysis of Fe-phases in drill-cores from the Triassic Stuttgart formation at Ketzin CO<sub>2</sub> storage site before CO<sub>2</sub> arrival. *Environ Earth Sci* 76(4):161
- Klein E, De Lucia M, Kempka T, Kühn M (2013) Evaluation of long-term mineral trapping at the Ketzin pilot site for CO<sub>2</sub> storage: an integrative approach using geochemical modelling and reservoir simulation. *Int J Greenhouse Gas Control* 19:720–730
- Kühn M, Stanjek H, Peiffer S, Clauser C (2013) Mineral trapping of CO<sub>2</sub> in operated geothermal reservoirs—numerical simulations on various scales. *Energy Procedia* 40:454–463
- Labus M, Wertz F (2017) Identifying geochemical reactions on well-bore cement/caprock interface under sequestration conditions. *Environ Earth Sci* 76(12):443
- Lattemann S, Höpner T (2008) Environmental impact and impact assessment of seawater desalination. *Desalination* 220(1):1–15
- Li J, Duan Z (2011) A thermodynamic model for the prediction of phase equilibria and speciation in the H<sub>2</sub>O–CO<sub>2</sub>–NaCl–CaCO<sub>3</sub>–CaSO<sub>4</sub> system from 0 to 250°C, 1 to 1000 bar with NaCl concentrations up to halite saturation. *Geochim Cosmochim Acta* 75(15):4351–4376
- Liebscher A, Möller F, Bannach A, Köhler S, Wiebach J, Schmidt-Hattenberger C, Weiner M, Pretschner C, Ebert K, Zemke J (2013) Injection operation and operational pressure–temperature monitoring at the CO<sub>2</sub> storage pilot site Ketzin, Germany—design, results, recommendations. *Int J Greenhouse Gas Control* 15:163–173
- Martens S, Möller F, Streibel M, Liebscher A (2014) Completion of five years of safe CO<sub>2</sub> injection and transition to the post-closure phase at the Ketzin pilot site. *Energy Procedia* 59:190–197
- Martens S, Kempka T, Liebscher A, Möller F, Schmidt-Hattenberger C, Streibel M, Szizybalski A, Zimmer M (2015) Field experiment on CO<sub>2</sub> back-production at the Ketzin pilot site. *Energy Procedia* 76:519–527
- Möller F, Liebscher A, Martens S, Schmidt-Hattenberger C, Kühn M (2012) Yearly operational datasets of the CO<sub>2</sub> storage pilot site Ketzin, Germany (Scientific Technical Report - Data ; 12/06). Potsdam, Deutsches GeoForschungsZentrum GFZ, 14 p. <https://doi.org/10.2312/GFZ.b103-12066>.
- Norden B, Frykman P (2013) Geological modelling of the Triassic Stuttgart formation at the Ketzin CO<sub>2</sub> storage site, Germany. *Int J Greenhouse Gas Control* 19:756–774
- Parkhurst DL, Appelo CAJ (2013) Description of input and examples for PHREEQC version 3—A computer program for speciation, batch-reaction, one-dimensional transport, and inverse geochemical calculations. U.S. Geological Survey Techniques and Methods, book 6, chap. A43. Available only at <https://pubs.usgs.gov/tm/06/a43/>
- Pitzer KS (1973) Thermodynamics of electrolytes. I. Theoretical basis and general equations. *J Phys Chem* 77(2):268–277
- Prevedel B, Wohlgemuth L, Legarth B, Henninges J, Schütt H, Schmidt-Hattenberger C, Norden B, Förster A, Hurter S (2009) The CO<sub>2</sub>SINK boreholes for geological CO<sub>2</sub>-storage testing. *Energy Procedia* 1(1):2087–2094
- Prevedel B, Martens S, Norden B, Henninges J, Freifeld BM (2014) Drilling and abandonment preparation of CO<sub>2</sub> storage wells—experience from the Ketzin pilot site. *Energy Procedia* 63:6067–6078
- Prinet C, Thibeau S, Lescanne M, Monne J (2013) Lacq-rousse CO<sub>2</sub> capture and storage demonstration pilot: lessons learnt from two and a half years monitoring. *Energy Procedia* 37:3610–3620
- Reiss AG, Gavrieli I, Rosenberg YO, Reznik II, Luttge A, Emmanuel S, Ganor J (2021) Gypsum precipitation under saline conditions: thermodynamics kinetics, morphology, and size distribution. *Minerals* 11(2):141
- Rendel PM, Gavrieli I, Wolff-Boenisch D, Ganor J (2016) Gypsum solubility under pressure conditions relevant to CO<sub>2</sub> geological storage. *Int J Greenhouse Gas Control* 55:15–22
- Reznik II, Gavrieli I, Antler G, Ganor J (2011) Kinetics of gypsum crystal growth from high ionic strength solutions: a case study of Dead sea—seawater mixtures. *Geochim Cosmochim Acta* 75(8):2187–2199
- Ringrose PS, Mathieson AS, Wright IW, Selama F, Hansen O, Bissell R, Saoula N, Midgley J (2013) The In Salah CO<sub>2</sub> storage project: lessons learned and knowledge transfer. *Energy Procedia* 37:6226–6236
- Rosenberg YO, Reznik II, Zmora-Nahum S, Ganor J (2012) The effect of pH on the formation of a gypsum scale in the presence of a phosphonate antiscale. *Desalination* 284:207–220
- Schmidt-Hattenberger C, Jurczyk C, Liebscher A, Möller F, Norden B, Prevedel B, Wiese B, Zemke K, Zimmer M (2018) Post-injection monitoring and well abandonment results of the Ketzin test site – an essential part for transfer of liability, in Proceedings 14th International Conference on Greenhouse Gas Control Technologies-GHGT-14, Melbourne, Australia
- Tremosa J, Castillo C, Vong CQ, Kervévan C, Lassin A, Audigane P (2014) Long-term assessment of geochemical reactivity of CO<sub>2</sub> storage in highly saline aquifers: application to Ketzin. In Salah and Snøhvit storage sites. *Int J Greenhouse Gas Control* 20:2–26
- Underschultz J, Boreham C, Dance T, Stalker L, Freifeld B, Kirste D, Ennis-King J (2011) CO<sub>2</sub> storage in a depleted gas field: an overview of the CO<sub>2</sub>CRC Otway project and initial results. *Int J Greenhouse Gas Control* 5(4):922–932
- Van Driessche AES, Stawski TM, Kellermeier M (2019) Calcium sulfate precipitation pathways in natural and engineered environments. *Chem Geol* 530:119274
- Wagner FM, Wiese BU (2018) Fully coupled inversion on a multi-physical reservoir model—part II: the Ketzin CO<sub>2</sub> storage reservoir. *Int J Greenhouse Gas Control* 75:273–281
- Wiese B, Böhner J, Enachescu C, Würdemann H, Zimmermann G (2010) Hydraulic characterisation of the Stuttgart formation at the pilot test site for CO<sub>2</sub> storage Ketzin, Germany. *Int J Greenhouse Gas Control* 4(6):960–971
- Wiese B, Zimmer M, Nowak M, Pellizzari L, Pilz PJEES (2013) Well-based hydraulic and geochemical monitoring of the above zone of the CO<sub>2</sub> reservoir at Ketzin, Germany. *Environ Earth Sci* 70(8):3709–3726
- Wipki M, Ivanova A, Liebscher A, Lüth S, Möller F, Szizybalski A, Wiese B, Zimmer M (2016) Monitoring concept for CO<sub>2</sub> storage at the Ketzin pilot site, Germany—post-injection continuation towards transfer of liability. *Energy Procedia* 97:348–355
- Wolfe WW, Bennett P (2011) Solubility and dissolution kinetics of gypsum as a function of CO<sub>2</sub> partial pressure: implications for geological carbon sequestration William Wolfe, Philip Bennett the University of Texas at Austin, Jackson School of geosciences. AGU Fall Meeting Abstr 2011:H51G-1267
- Würdemann H, Möller F, Kühn M, Heidug W, Christensen NP, Borm G, Schilling FR (2010) CO<sub>2</sub>SINK—from site characterisation and risk assessment to monitoring and verification: One year of operational experience with the field laboratory for CO<sub>2</sub> storage at Ketzin, Germany. *Int J Greenhouse Gas Control* 4(6):938–951
- Xu T, Apps JA, Pruess K (2003) Reactive geochemical transport simulation to study mineral trapping for CO<sub>2</sub> disposal in deep arenaceous formations. *J Geophys Res Solid Earth* 108:B2

**Publisher's Note** Springer Nature remains neutral with regard to jurisdictional claims in published maps and institutional affiliations.